

Research Paper

Effects of Three-Axial Material Inhomogeneity on Lengthwise Cracks in Non-Linear Elastic Beams

Victor Iliev RIZOV

*Department of Technical Mechanics
University of Architecture, Civil Engineering and Geodesy*

1 Chr. Smirnensky blvd., 1046 – Sofia, Bulgaria
e-mail: v_rizov_fhe@uacg.bg

The present paper investigates lengthwise crack behaviour in three-axial inhomogeneous non-linear elastic cantilever beams, i.e., beams which exhibit inhomogeneous material properties along the width, height and length. The non-linear mechanical behaviour of the inhomogeneous material is described by the Ramberg-Osgood equation assuming that the modulus of elasticity varies linearly along the width, height and length of beams. A solution to the strain energy release rate is derived by considering the balance of the energy. The results obtained in the present paper indicate that the three-axial inhomogeneous material properties have a significant influence on the strain energy release rate in non-linear elastic beams.

Key words: three-axial inhomogeneous beam; lengthwise crack; non-linear mechanical behaviour of the material.

1. INTRODUCTION

An adequate crack analysis in inhomogeneous engineering structures is very important for the evaluation of their integrity, reliability and durability. Developing techniques for such analyses requires consideration of various physical features. One of the most important features is the fact that the properties of inhomogeneous materials depend on the location, i.e., the properties are functions of the coordinates [1–3]. It should be noted that the growing interest towards the inhomogeneous materials is due mainly to the increasing application of functionally graded materials and structures in aeronautics, nuclear reactors, electronics, energy sector, biomedicine, etc. [4–6]. For the last decades, the functionally graded materials have attracted the attention mostly because their properties can be varied smoothly along one or more spatial coordinates during manufacturing so as to optimise the reaction of functionally graded structural members and components to the externally applied mechanical loads and influences.

The dependences of material properties on the coordinates significantly complicate the fracture analysis of inhomogeneous structures in comparison with the structures made of traditional homogeneous structural materials. Another important physical feature that should be taken into account in fracture analyses is the non-linear mechanical behaviour of the inhomogeneous materials. Recently, several papers which deal with a lengthwise fracture in inhomogeneous (functionally graded) beam structures exhibiting material non-linearity have been published [7–9]. The material non-linearity was described by using power law stress-strain relations. It was assumed that the coefficient in the power law stress-strain relation varies continuously along the beam height, i.e., the beam exhibits material inhomogeneity in height direction only [7, 8]. Additionally, analyses of lengthwise crack in non-linear elastic beam configurations were performed assuming that the coefficient in the power law stress-strain relation varies in both height and width directions of the beam (the coefficient is distributed symmetrically with respect to the vertical centroidal axis of the beam cross-section) [9]. Non-linear solutions to the strain energy release rate were derived by analysing the complementary strain energy cumulated in the beams [7–9].

The present paper aims to develop a lengthwise crack analysis of a non-linear elastic cantilever beam which exhibits smooth three-axial material inhomogeneity (it is assumed that the modulus of elasticity is distributed linearly along the width, height and length of the beam). The non-linear mechanical behaviour of the inhomogeneous material is described by applying the Ramberg-Osgood stress-strain relation. The crack is studied in terms of the strain energy release rate by considering the energy balance. It should be mentioned that the crack analysis developed in the present paper holds for non-linear elastic behaviour of the material. The analysis is also applicable for elastic-plastic behaviour if the beam undergoes active deformation, i.e., if the external loading increases only [10].

2. STUDY OF THE STRAIN ENERGY RELEASE RATE

A lengthwise crack of length a is located in the mid-plane of the inhomogeneous beam configuration shown in Fig. 1. Here, it should be mentioned that one of the motives for the present study is that certain kinds of inhomogeneous materials, such as functionally graded materials, can be built up layer by layer [5], which is a premise for the appearance of lengthwise cracks between layers. The cross-section of the beam is a rectangle of width b , and height $2h$. The length of the beam is denoted by l . The beam is clamped in section $K_2S_2T_2$. The external loading consists of two bending moments M_L and M_U applied at the free ends of the lower and upper crack arms, respectively (Fig. 1). The beam under consideration exhibits inhomogeneous material properties along the width, height

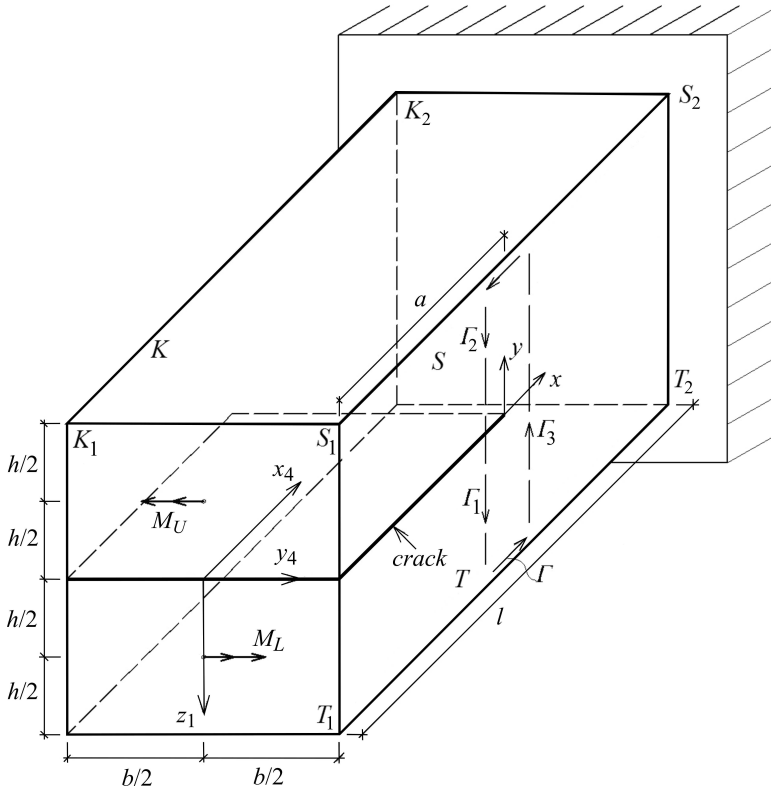


FIG. 1. Geometry and loading of a three-axial inhomogeneous non-linear elastic cantilever beam containing a lengthwise crack.

and length (it is assumed that the modulus of elasticity varies linearly along the width, height and length of the beam). Besides, it is assumed that the beam exhibits non-linear mechanical behaviour of the material which is described by using the Ramberg-Osgood stress-strain relation.

The lengthwise crack is studied in terms of the strain energy release rate G , by analysing the energy balance. Assuming a small increase δa of the crack length, the energy balance is written as

$$(2.1) \quad M_L \delta \varphi_L + M_U \delta \varphi_U = \frac{\partial U}{\partial a} \delta a + G b \delta a,$$

where φ_L and φ_U are, respectively, the angles of rotation of the free ends of the lower and upper crack arms, U is the strain energy. From (2.1), one obtains

$$(2.2) \quad G = \frac{M_L}{b} \frac{\partial \varphi_L}{\partial a} + \frac{M_U}{b} \frac{\partial \varphi_U}{\partial a} - \frac{1}{b} \frac{\partial U}{\partial a}.$$

By applying the Castigliano's theorem for structures exhibiting material non-linearity, φ_L and φ_U are written as

$$(2.3) \quad \varphi_L = \frac{\partial U^*}{\partial M_L},$$

$$(2.4) \quad \varphi_U = \frac{\partial U^*}{\partial M_U},$$

where U^* is the complementary strain energy.

The strain energy cumulated in the beam is obtained as

$$(2.5) \quad U = U_L + U_U + U_R,$$

where U_L , U_U , and U_R are, respectively, the strain energies in the lower and upper crack arms, and the uncracked beam portion, $a \leq x_4 \leq l$ (Fig. 1).

The strain energy in the lower crack arm is expressed as

$$(2.6) \quad U_L = \int_0^a \int_{-\frac{b}{2}}^{\frac{b}{2}} \int_{-\frac{h}{2}}^{\frac{h}{2}} u_{0L} dx_4 dy_1 dz_1,$$

where u_{0L} is the strain energy density in the lower crack arm, and y_1 and z_1 are the centroidal axes of the lower crack arm (Fig. 2).

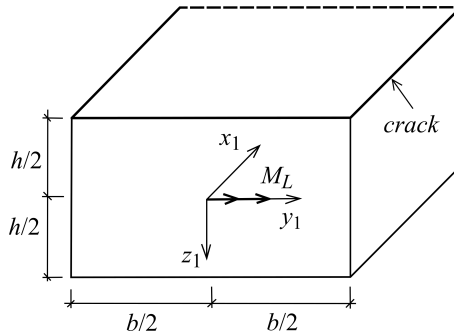


FIG. 2. Free end of the lower crack arm.

Analogically, the strain energies in the upper crack arm and the uncracked beam portion are written, respectively, as

$$(2.7) \quad U_U = \int_0^a \int_{-\frac{b}{2}}^{\frac{b}{2}} \int_{-\frac{h}{2}}^{\frac{h}{2}} u_{0U} dx_4 dy_2 dz_2$$

and

$$(2.8) \quad U_R = \int_a^l \int_{-\frac{b}{2}}^{\frac{b}{2}} \int_{-h}^h u_{0R} dx_4 dy_3 dz_3,$$

where u_{0U} and u_{0R} are the strain energy densities in the upper crack arm and the un-cracked beam portion, respectively.

Similarly to formulae (2.5)–(2.8), the complementary strain energy cumulated in the beam is obtained as

$$(2.9) \quad U^* = \int_0^a \int_{-\frac{b}{2}}^{\frac{b}{2}} \int_{-\frac{h}{2}}^{\frac{h}{2}} u_{0L}^* dx_4 dy_1 dz_1 + \int_0^a \int_{-\frac{b}{2}}^{\frac{b}{2}} \int_{-\frac{h}{2}}^{\frac{h}{2}} u_{0U}^* dx_4 dy_2 dz_2 \\ + \int_a^l \int_{-\frac{b}{2}}^{\frac{b}{2}} \int_{-h}^h u_{0R}^* dx_4 dy_3 dz_3,$$

where u_{0L}^* , u_{0U}^* , and u_{0R}^* are the complementary strain energy densities in the lower and upper crack arms, and the uncracked beam portion, respectively.

The Ramberg-Osgood stress-strain relation that is used to describe the non-linear mechanical behaviour of the material is written as

$$(2.10) \quad \varepsilon = \frac{\sigma}{E} + \left(\frac{\sigma}{H} \right)^{\frac{1}{n}},$$

where ε is the lengthwise strain, σ is the normal stress, E is the modulus of elasticity, H and n are material properties. The modulus of elasticity varies continuously in the beam cross-section according to the following linear law [11]:

$$(2.11) \quad E = q_1 y_4 + q_2 z_4 + q_3,$$

where

$$(2.12) \quad -\frac{b}{2} \leq y_4 \leq \frac{b}{2},$$

$$(2.13) \quad -h \leq z_4 \leq h.$$

In (2.11),

$$(2.14) \quad q_1 = \frac{1}{b} (E_S - E_K),$$

$$(2.15) \quad q_2 = \frac{1}{h} (E_T - E_S),$$

$$(2.16) \quad q_3 = \frac{1}{2} (E_T + E_K),$$

where E_K , E_S , and E_T are, respectively, the values of the modulus of elasticity in points K , S , and T in an arbitrary cross-section KST of the beam (Fig. 1). Besides, it is assumed that E_K , E_S , and E_T vary linearly along the beam length

$$(2.17) \quad E_K = E_{K_1} + \frac{E_{K_2} - E_{K_1}}{l} x_4,$$

$$(2.18) \quad E_S = E_{S_1} + \frac{E_{S_2} - E_{S_1}}{l} x_4,$$

$$(2.19) \quad E_T = E_{T_1} + \frac{E_{T_2} - E_{T_1}}{l} x_4,$$

where

$$(2.20) \quad 0 \leq x_4 \leq l.$$

In (2.17), (2.18) and (2.19), E_{K_1} , E_{S_1} , and E_{T_1} are, respectively, the values of E_K , E_S , and E_T in points K_1 , S_1 , and T_1 at the free end of the beam, E_{K_2} , E_{S_2} , and E_{T_2} are, respectively, the values of E_K , E_S , and E_T in points K_2 , S_2 , and T_2 at the clamped end of the beam (Fig. 1). It can be summarised that formulae (2.11)–(2.20) describe the continuous variation of the modulus of elasticity in the inhomogeneous cantilever beam configuration (Fig. 1).

In principle, the strain energy density is equal to the area OPQ enclosed by the stress-strain curve (Fig. 3). For the Ramberg-Osgood stress-strain relation, the strain energy density in the lower crack arm is expressed as [12]

$$(2.21) \quad u_{0L} = \frac{\sigma^2}{2E_L} + \frac{\sigma^{\frac{1+n}{n}}}{(1+n)H^{\frac{1}{n}}},$$

where σ and E_L are, respectively, the distributions of the normal stresses and the modulus of elasticity in the lower crack arm cross-section. By using (2.11), the distribution of the modulus of elasticity in the lower crack arm cross-section is written as

$$(2.22) \quad E_L = q_1 y_1 + q_2 z_1 + q_3 L,$$

where

$$(2.23) \quad q_{3L} = q_2 \frac{h}{2} + q_3,$$

$$(2.24) \quad -\frac{b}{2} \leq y_1 \leq \frac{b}{2},$$

$$(2.25) \quad -\frac{h}{2} \leq z_1 \leq \frac{h}{2}.$$

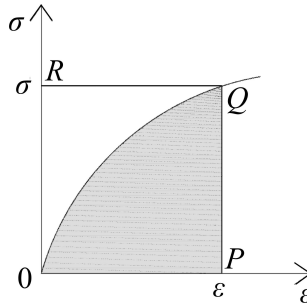


FIG. 3. Non-linear stress-strain curve.

By substituting of (2.22) in (2.21), one arrives at

$$(2.26) \quad u_{0L} = \frac{\sigma^2}{2(q_1 y_1 + q_2 z_1 + q_{3L})} + \frac{\sigma^{\frac{1+n}{n}}}{(1+n)H^{\frac{1}{n}}}.$$

Formula (2.26) is used also to obtain the strain energy density in the upper crack arm. For this purpose, σ is replaced with the distribution of the normal stresses σ_U in the upper crack arm. Also, q_{3L} is replaced with q_{3U} where q_{3U} is obtained by the following formula:

$$(2.27) \quad q_{3U} = -q_2 \frac{h}{2} + q_3.$$

The strain energy density in the uncracked beam portion is determined by (2.26) by replacing of σ with the distribution of the normal stresses in uncracked beam portion σ_R . In addition, q_{3L} is replaced with q_3 .

The complementary strain energy density is equal to the area OQR that supplements the area OPQ , to a rectangle (Fig. 3). Therefore, the complementary strain energy density in the lower crack arm is written as

$$(2.28) \quad u_{0L}^* = \sigma \varepsilon - u_{0L}.$$

By substituting of (2.10) and (2.26) in (2.28), one derives

$$(2.29) \quad u_{0L}^* = \frac{\sigma^2}{2(q_1 y_1 + q_2 z_1 + q_{3L})} + \frac{n\sigma^{\frac{1+n}{n}}}{(1+n)H^{\frac{1}{n}}}.$$

Formula (2.29) is also applied to determine the complementary strain energy density in the upper crack arm. For this purpose, σ and q_{3L} are replaced with the σ_U and q_{3U} , respectively. Similarly, the complementary strain energy density in the un-cracked beam portion is derived by replacing of σ and q_{3L} , respectively, with σ_R and q_3 in (2.29).

In order to perform the integration in (2.6), σ has to be expressed as a function of y_1 and z_1 . However, it is obvious that σ cannot be determined explicitly from the Ramberg-Osgood equation (2.10). Therefore, σ is expanded in the series of Maclaurin by keeping the first six members

$$(2.30) \quad \sigma(y_1, z_1) \approx \sigma(0, 0) + \frac{\partial\sigma(0, 0)}{\partial y_1} y_1 + \frac{\partial\sigma(0, 0)}{\partial z_1} z_1 + \frac{\partial^2\sigma(0, 0)}{2!\partial y_1^2} y_1^2 \\ + \frac{\partial^2\sigma(0, 0)}{\partial y_1 \partial z_1} y_1 z_1 + \frac{\partial^2\sigma(0, 0)}{2!\partial z_1^2} z_1^2.$$

Formula (2.30) is rewritten as

$$(2.31) \quad \sigma(y_1, z_1) \approx \beta_1 + \beta_2 y_1 + \beta_3 z_1 + \beta_4 y_1^2 + \beta_5 y_1 z_1 + \beta_6 z_1^2,$$

where the coefficients, β_1 , β_2 , β_3 , β_4 , β_5 , and β_6 , are determined in the following way. First, the distribution of the lengthwise strains in the lower crack arm cross-section is analysed. The validity of the Bernoulli hypothesis for plane sections is assumed since the span to height ratio of the beam under consideration is large. Thus, ε written as

$$(2.32) \quad \varepsilon = \varepsilon_{C_1} + \kappa_{y_1} y_1 + \kappa_{z_1} z_1,$$

where ε_{C_1} is the strain in the centre of the lower crack arm cross-section, and κ_{y_1} and κ_{z_1} are the curvatures the of lower crack arm in the $x_1 y_1$ and $x_1 z_1$ planes, respectively. Concerning the applicability of the Bernoulli hypothesis, it should also be noted that since the beam is loaded in pure bending, the only non-zero strain is ε . Thus, according to the small strains compatibility equations, ε is distributed linearly in the cross-section of the lower crack arm. It should be mentioned that the Bernoulli hypothesis has already been used in longitudinal fracture analyses of inhomogeneous beam configurations [13].

Further, formulae (2.22), (2.31) and (2.32) are substituted in (2.10)

$$(2.33) \quad \varepsilon_{C_1} + \kappa_{y_1} y_1 + \kappa_{z_1} z_1 = \frac{\beta_1 + \beta_2 y_1 + \beta_3 z_1 + \beta_4 y_1^2 + \beta_5 y_1 z_1 + \beta_6 z_1^2}{q_1 y_1 + q_2 z_1 + q_{3L}} + \frac{(\beta_1 + \beta_2 y_1 + \beta_3 z_1 + \beta_4 y_1^2 + \beta_5 y_1 z_1 + \beta_6 z_1^2)^{\frac{1}{n}}}{H^{\frac{1}{n}}}.$$

By substituting of $y_1 = 0$ and $z_1 = 0$ in (2.33), one arrives at

$$(2.34) \quad \varepsilon_{C_1} = \frac{\beta_1}{q_{3L}} + \frac{\beta_1^{\frac{1}{n}}}{H^{\frac{1}{n}}}.$$

Then, by substituting of $y_1 = 0$ and $z_1 = 0$ in the first derivative of (2.33) with respect to y_1 , one obtains

$$(2.35) \quad \kappa_{y_1} q_{3L} + \varepsilon_{C_1} q_1 = \beta_2 + \frac{1}{H^{\frac{1}{n}}} \left(q_1 \beta_1^{\frac{1}{n}} + q_{3L} \frac{1}{n} \beta_1^{\frac{1}{n}-1} \beta_2 \right).$$

Similarly, by substituting of $y_1 = 0$ and $z_1 = 0$ in the first derivative of (2.33) with respect to z_1 , one arrives at

$$(2.36) \quad \kappa_{z_1} q_{3L} + \varepsilon_{C_1} q_2 = \beta_3 + \frac{1}{H^{\frac{1}{n}}} \left(q_2 \beta_1^{\frac{1}{n}} + q_{3L} \frac{1}{n} \beta_1^{\frac{1}{n}-1} \beta_3 \right).$$

Furthermore, by substituting of $y_1 = 0$ and $z_1 = 0$ in the second derivative of (2.33) with respect to y_1 , in the second mixed derivative of (2.33) and in the second derivative of (2.33) with respect to z_1 , one obtains

$$(2.37) \quad 2\kappa_{y_1} q_1 = 2\beta_4 + \frac{1}{H^{\frac{1}{n}}} \left\{ q_1 \frac{1}{n} \beta_1^{\frac{1}{n}-1} \beta_2 + q_1 \frac{1}{n} \beta_1^{\frac{1}{n}-1} \beta_2 + \left[\frac{2}{n} \beta_4 \beta_1^{\frac{1}{n}-1} + \beta_2 \frac{1}{n} \left(\frac{1}{n} - 1 \right) \beta_1^{\frac{1}{n}-2} \beta_2 \right] \right\},$$

$$(2.38) \quad \kappa_{y_1} q_2 + \kappa_{z_1} q_1 = \beta_5 + \frac{1}{H^{\frac{1}{n}}} \left\{ q_1 \frac{1}{n} \beta_1^{\frac{1}{n}-1} \beta_3 + q_2 \frac{1}{n} \beta_1^{\frac{1}{n}-1} \beta_2 + q_{3L} \left[\beta_5 \frac{1}{n} \beta_1^{\frac{1}{n}-1} + \beta_2 \frac{1}{n} \left(\frac{1}{n} - 1 \right) \beta_1^{\frac{1}{n}-2} \beta_3 \right] \right\},$$

$$(2.39) \quad 2\kappa_{z_1} q_2 = 2\beta_6 + \frac{1}{H^{\frac{1}{n}}} \left[q_2 \frac{1}{n} \beta_1^{\frac{1}{n}-1} \beta_3 + q_2 \frac{1}{n} \beta_1^{\frac{1}{n}-1} \beta_3 + q_{3L} \frac{1}{n} \left(\frac{1}{n} - 1 \right) \beta_1^{\frac{1}{n}-2} \beta_3^2 + 2\beta_1^{\frac{1}{n}-1} \beta_6 \right].$$

There are nine unknowns, $\beta_1, \beta_2, \beta_3, \beta_4, \beta_5, \beta_6, \varepsilon_{C_1}, \kappa_{y_1}$, and κ_{z_1} , in Eqs (2.34)–(3.39). Three other equations are derived by considering the equilibrium of the elementary forces in the cross-section of the lower crack arm

$$(2.40) \quad N = \iint_{A_1} \sigma \, dA,$$

$$(2.41) \quad M_{y_1} = \iint_{A_1} \sigma z_1 \, dA,$$

$$(2.42) \quad M_{z_1} = \iint_{A_1} \sigma y_1 \, dA,$$

where A_1 is the area of the lower crack arm cross-section, N , M_{y_1} , and M_{z_1} are, respectively, the axial force and the bending moments about the centroidal axes, y_1 and z_1 . It is obvious that (Fig. 2)

$$(2.43) \quad N = 0,$$

$$(2.44) \quad M_{y_1} = M_L,$$

$$(2.45) \quad M_{z_1} = 0.$$

By substituting of (2.31) in (2.40)–(2.42), one derives

$$(2.46) \quad N = \beta_1 b h + \beta_4 \frac{b^3 h}{12} + \beta_6 \frac{b h^3}{12},$$

$$(2.47) \quad M_{y_1} = \beta_3 \frac{b h^3}{12},$$

$$(2.48) \quad M_{z_1} = \beta_2 \frac{b^3 h}{12}.$$

Equations (2.34)–(2.39) and (2.46)–(2.48) should be solved with respect to $\beta_1, \beta_2, \beta_3, \beta_4, \beta_5, \beta_6, \varepsilon_{C_1}, \kappa_{y_1}$, and κ_{z_1} by using the MatLab computer program. It should be noted that Eqs (2.34)–(2.39) and (2.46)–(2.48) can be applied to determine $\beta_1, \beta_2, \beta_3, \beta_4, \beta_5, \beta_6, \varepsilon_{C_1}, \kappa_{y_1}$, and κ_{z_1} at any cross-section of the lower crack arm, i.e., for any x_4 in the interval $[0; a]$ (the only difference between the various cross-sections are the values of E_K, E_S , and E_T which are obtained by formulae (2.17)–(2.19)).

Equations (2.34)–(2.39) and (2.46)–(2.48) are applied also to obtain $\beta_{U1}, \beta_{U2}, \beta_{U3}, \beta_{U4}, \beta_{U5}, \beta_{U6}, \varepsilon_{C_2}, \kappa_{y_2}$, and κ_{z_2} at the cross-section of the upper crack arm (here, ε_{C_2} is the strain in the centre of the upper crack arm cross-section, κ_{y_2} and κ_{z_2} are, respectively, the curvatures of the upper crack arm in the $x_2 y_2$ and $x_2 z_2$ planes). For this purpose, $\beta_1, \beta_2, \beta_3, \beta_4, \beta_5, \beta_6, q_{3L}, \varepsilon_{C_1}, \kappa_{y_1}$, and κ_{z_1} are

replaced, respectively, with $\beta_{U1}, \beta_{U2}, \beta_{U3}, \beta_{U4}, \beta_{U5}, \beta_{U6}, q_{3U}, \varepsilon_{C2}, \kappa_{y2}$, and κ_{z2} in Eqs (2.34)–(2.39) and (2.46)–(2.48). Additionally, M_{y1} is replaced with M_U (Fig. 1). The stress σ_U , in the upper crack arm cross-section, is determined by replacing of $\beta_1, \beta_2, \beta_3, \beta_4, \beta_5, \beta_6, y_1$, and z_1 , respectively, with $\beta_{U1}, \beta_{U2}, \beta_{U3}, \beta_{U4}, \beta_{U5}, \beta_{U6}, y_2$, and z_2 in (2.31).

Analogically, the parameters, $\beta_{R1}, \beta_{R2}, \beta_{R3}, \beta_{R4}, \beta_{R5}, \beta_{R6}, \varepsilon_{C3}, \kappa_{y3}$, and κ_{z3} , of the cross-section of the uncracked beam portion are obtained by replacing of $\beta_1, \beta_2, \beta_3, \beta_4, \beta_5, \beta_6, q_{3L}, \varepsilon_{C1}, \kappa_{y1}$, and κ_{z1} , respectively, with $\beta_{R1}, \beta_{R2}, \beta_{R3}, \beta_{R4}, \beta_{R5}, \beta_{R6}, q_3, \varepsilon_{C3}, \kappa_{y3}$, and κ_{z3} in Eqs (2.34)–(2.39) and (2.46)–(2.48). Also, h and M_{y1} are replaced, respectively, with $2h$ and $M_U - M_L$ (Fig. 1). Formula (2.31) is applied to calculate the stress σ_R in the uncracked beam portion. For this purpose, $\beta_1, \beta_2, \beta_3, \beta_4, \beta_5, \beta_6, y_1$, and z_1 are replaced with $\beta_{R1}, \beta_{R2}, \beta_{R3}, \beta_{R4}, \beta_{R5}, \beta_{R6}, y_2$, and z_2 , respectively.

By substituting of (2.3)–(2.8) and (2.9) in (2.2), one arrives at

(2.49)

$$G = \frac{M_L}{b} \frac{\partial}{\partial M_L} \left(\int_{-\frac{b}{2}}^{\frac{b}{2}} \int_{-\frac{h}{2}}^{\frac{h}{2}} u_{0L}^* dy_1 dz_1 + \int_{-\frac{b}{2}}^{\frac{b}{2}} \int_{-\frac{h}{2}}^{\frac{h}{2}} u_{0U}^* dy_2 dz_2 - \int_{-\frac{b}{2}}^{\frac{b}{2}} \int_{-h}^h u_{0R}^* dy_3 dz_3 \right) \\ + \frac{M_U}{b} \frac{\partial}{\partial M_U} \left(\int_{-\frac{b}{2}}^{\frac{b}{2}} \int_{-\frac{h}{2}}^{\frac{h}{2}} u_{0L}^* dy_1 dz_1 + \int_{-\frac{b}{2}}^{\frac{b}{2}} \int_{-\frac{h}{2}}^{\frac{h}{2}} u_{0U}^* dy_2 dz_2 - \int_{-\frac{b}{2}}^{\frac{b}{2}} \int_{-h}^h u_{0R}^* dy_3 dz_3 \right) \\ - \frac{1}{b} \left(\int_{-\frac{b}{2}}^{\frac{b}{2}} \int_{-\frac{h}{2}}^{\frac{h}{2}} u_{0L} dy_1 dz_1 + \int_{-\frac{b}{2}}^{\frac{b}{2}} \int_{-\frac{h}{2}}^{\frac{h}{2}} u_{0U} dy_2 dz_2 - \int_{-\frac{b}{2}}^{\frac{b}{2}} \int_{-h}^h u_{0R} dy_3 dz_3 \right),$$

where $u_{0L}, u_{0U}, u_{0R}, u_{0L}^*, u_{0U}^*$, and u_{0R}^* are determined by (2.26), (2.29), (2.31), (2.34)–(2.39), and (2.46)–(2.48) at $x_4 = a$. The integration in (2.49) should be performed by the MatLab computer program. The derivatives $\frac{\partial}{\partial M_L}(\dots)$ and $\frac{\partial}{\partial M_U}(\dots)$ in (2.49) should be determined numerically by the MatLab computer program.

In order to verify (2.49), the strain energy release rate is also derived by using the following formula [8]:

$$(2.50) \quad G = \frac{dU^*}{bda},$$

where dU^* is the change of the complementary strain energy, and da is an elementary increase of the crack length. By substituting of (2.9) in (2.50), one obtains

$$(2.51) \quad G = \frac{1}{b} \left(\int_{-\frac{b}{2}}^{\frac{b}{2}} \int_{-\frac{h}{2}}^{\frac{h}{2}} u_{0L}^* dy_1 dz_1 + \int_{-\frac{b}{2}}^{\frac{b}{2}} \int_{-\frac{h}{2}}^{\frac{h}{2}} u_{0U}^* dy_2 dz_2 - \int_{-\frac{b}{2}}^{\frac{b}{2}} \int_{-h}^h u_{0R}^* dy_3 dz_3 \right),$$

where u_{0L}^* , u_{0U}^* , and u_{0R}^* are determined by (2.29), (2.31), (2.34)–(2.39) and (2.46)–(2.48) at $x_4 = a$. The integration in (2.51) should be performed by the MatLab computer program. The strain energy release rates calculated by (2.51) are the exact matches of the strain energy release rates obtained by (2.50). This fact is a verification of the crack analysis developed in the present paper. It should be noted that the strain energy release rate is also analysed by keeping more than six members in the series of Maclaurin (2.30). The results obtained are very close to those derived by keeping the first six members (the difference is less than 2%).

Due to the material inhomogeneity, the strain energy release rate is distributed non-uniformly along the crack front. It should be mentioned that formulae (2.50) and (2.51) calculate the average value of the strain energy release rate along the crack front. Therefore, in order to evaluate the distribution of the strain energy release rate along the crack front the crack is also analysed by applying the J -integral approach since the J -integral is equal to the strain energy release rate [7].

The J -integral is solved along the contour Γ shown as a dashed line in Fig. 1. Thus, the J -integral solution is written as

$$(2.52) \quad J = J_{\Gamma_1} + J_{\Gamma_2} + J_{\Gamma_3},$$

where J_{Γ_1} , J_{Γ_2} , and J_{Γ_3} are the J -integral values, respectively, in segments, Γ_1 , Γ_2 , and Γ_3 , of the integration contour. The J -integral in segment Γ_1 is written as

$$(2.53) \quad J_{\Gamma_1} = \int_{\Gamma_1} \left[u_{0L} \cos \alpha - \left(p_x \frac{\partial u}{\partial x} + p_y \frac{\partial v}{\partial x} \right) \right] ds_{\Gamma},$$

where the angle between the outwards normal vector to the contour of integration and the crack direction is marked by α , the components of the stress vector are marked by p_x and p_y , the components of the displacement vector with respect to the coordinate system xy are marked by u and v , and ds_{Γ} is a differential element along the contour of integration. The components of (2.53) are written as

$$(2.54) \quad p_x = -\sigma,$$

$$(2.55) \quad p_y = 0,$$

$$(2.56) \quad ds_{\Gamma} = dz_1,$$

$$(2.57) \quad \frac{\partial u}{\partial x} = \varepsilon,$$

$$(2.58) \quad \cos \alpha = -1.$$

By substituting of (2.54)–(2.58) in (2.53), one derives

$$(2.59) \quad J_{\Gamma_1} = \beta_1 \varepsilon_{C_1} h + \varepsilon_{C_1} \beta_6 \frac{h^3}{12} + \kappa_{z_1} \beta_3 \frac{h^3}{12} - \frac{\beta_1^2}{2q_{3L}} h - \frac{\beta_1^{\frac{1+n}{n}}}{(1+n) H^{\frac{1}{n}}} h \\ + \left(\beta_2 \varepsilon_{C_1} h + \kappa_{y_1} \beta_1 h + \kappa_{y_1} \beta_6 \frac{h^3}{12} + \kappa_{z_1} \beta_5 \frac{h^3}{12} \right) y_1 \\ + (\beta_4 \varepsilon_{C_1} h + \kappa_{y_1} \beta_2 h) y_1^2 + \kappa_{y_1} \beta_4 h y_1^3,$$

where

$$(2.60) \quad -\frac{b}{2} \leq y_1 \leq \frac{b}{12}.$$

The J -integral solution in segment Γ_2 of the integration contour (Fig. 1) can be found by using (2.59). For this purpose, $\beta_1, \beta_2, \beta_3, \beta_4, \beta_5, \beta_6, q_{3L}, \varepsilon_{C_1}, \kappa_{y_1}$, and κ_{z_1} are replaced with $\beta_{U1}, \beta_{U2}, \beta_{U3}, \beta_{U4}, \beta_{U5}, \beta_{U6}, q_{3U}, \varepsilon_{C_2}, \kappa_{y_2}$, and κ_{z_2} , respectively. Formula (2.59) is applied also to obtain the J -integral solution in segment Γ_3 of the integration contour. For this purpose, $h, \beta_1, \beta_2, \beta_3, \beta_4, \beta_5, \beta_6, q_{3L}, \varepsilon_{C_1}, \kappa_{y_1}$, and κ_{z_1} are replaced, respectively, with $2h, \beta_{R1}, \beta_{R2}, \beta_{R3}, \beta_{R4}, \beta_{R5}, \beta_{R6}, q_3, \varepsilon_{C_3}, \kappa_{y_3}$, and κ_{z_3} . Besides, the sign of (2.59) is set to “minus” since the contour of integration is directed upwards in segment Γ_3 .

By substituting of $J_{\Gamma_1}, J_{\Gamma_2}$ and J_{Γ_3} in (2.52), one obtains the following solution of the J -integral:

$$(2.61) \quad J = \beta_1 \varepsilon_{C_1} h + \varepsilon_{C_1} \beta_6 \frac{h^3}{12} + \kappa_{z_1} \beta_3 \frac{h^3}{12} - \frac{\beta_1^2}{2q_{3L}} h - \frac{\beta_1^{\frac{1+n}{n}}}{(1+n) H^{\frac{1}{n}}} h \\ + \left(\beta_2 \varepsilon_{C_1} h + \kappa_{y_1} \beta_1 h + \kappa_{y_1} \beta_6 \frac{h^3}{12} + \kappa_{z_1} \beta_5 \frac{h^3}{12} \right) y_1 + (\beta_4 \varepsilon_{C_1} h + \kappa_{y_1} \beta_2 h) y_1^2 \\ + \kappa_{y_1} \beta_4 h y_1^3 + \beta_{U1} \varepsilon_{C_2} h + \varepsilon_{C_2} \beta_{U6} \frac{h^3}{12} + \kappa_{z_2} \beta_{U3} \frac{h^3}{12} - \frac{\beta_{U1}^2}{2q_{3U}} h - \frac{\beta_{U1}^{\frac{1+n}{n}}}{(1+n) H^{\frac{1}{n}}} h \\ + \left(\beta_{U2} \varepsilon_{C_2} h + \kappa_{y_2} \beta_{U1} h + \kappa_{y_2} \beta_{U6} \frac{h^3}{12} + \kappa_{z_2} \beta_{U5} \frac{h^3}{12} \right) y_1 + (\beta_{U4} \varepsilon_{C_2} h + \kappa_{y_2} \beta_{U2} h) y_1^2 \\ + \kappa_{y_2} \beta_{U4} h y_1^3 - 2\beta_{R1} \varepsilon_{C_3} h - \varepsilon_{C_3} \beta_{R6} \frac{2h^3}{3} - \kappa_{z_3} \beta_{R3} \frac{2h^3}{3} + \frac{\beta_{R1}^2}{q_3} h + \frac{2\beta_{R1}^{\frac{1+n}{n}}}{(1+n) H^{\frac{1}{n}}} h \\ - \left(2\beta_{R2} \varepsilon_{C_3} h + 2\kappa_{y_3} \beta_{R1} h + \kappa_{y_3} \beta_{R6} \frac{2h^3}{3} + \kappa_{z_3} \beta_{R5} \frac{2h^3}{3} \right) y_1 \\ - (2\beta_{R4} \varepsilon_{C_3} h + 2\kappa_{y_3} \beta_{R2} h) y_1^2 + 2\kappa_{y_3} \beta_{R4} h y_1^3.$$

Formula (2.61) expresses the distribution of the J -integral value along the crack front.

The average value of the J -integral along the crack front is written as

$$(2.62) \quad J_{AV} = \frac{1}{b} \int_{-\frac{b}{2}}^{\frac{b}{2}} J dy_1.$$

It should be noted that the average value of the J -integral along the crack front obtained by substituting of (2.61) in (2.62) and performing the integration by the MatLab computer program is an exact match of the strain energy release rate. This fact is also a verification of the analysis developed in the present paper.

3. PARAMETRIC INVESTIGATION

A parametric investigation is carried out in order to evaluate the effects of three-axial material inhomogeneity and non-linear mechanical behaviour of the material on the lengthwise crack in the cantilever beam (Fig. 1). For this purpose, calculations of the strain energy release rate are performed by using (2.49). The results obtained are presented in non-dimensional form by using the formula $G_N = G / (E_{K_1} b)$. The material inhomogeneities along the width and height of the beam are characterised by E_{S_1}/E_{K_1} and E_{T_1}/E_{K_1} ratios, respectively. It is assumed that $b = 0.004$ m, $h = 0.004$ m, $l = 0.35$ m, $M_L = 0.40$ N·m, $M_U = 0.30$ N·m. Function (2.11) is written as $E = -9000y_4 + 33000z_4 + 168$ at $E_{S_1}/E_{K_1} = 0.7$, $E_{T_1}/E_{K_1} = 1.8$, $x_4 = 0.0$, and $E_{K_1} = 120$ GPa.

The strain energy release rate in non-dimensional form is plotted against E_{S_1}/E_{K_1} ratio in Fig. 4 at $a/l = 0.75$, $E_{T_1}/E_{K_1} = 0.6$, $H/E_{K_1} = 0.5$, $E_{K_2}/E_{K_1} =$

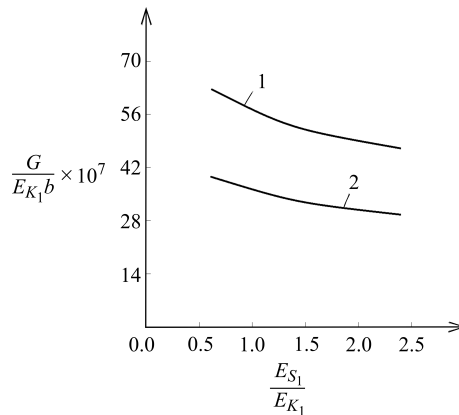


FIG. 4. The strain energy release rate in non-dimensional form presented as a function of E_{S_1}/E_{K_1} ratio (curve 1 – at non-linear mechanical behaviour of the material, curve 2 – at linear-elastic behaviour of the material).

0.5, $E_{S_2}/E_{S_1} = 0.5$, $E_{T_2}/E_{T_1} = 0.5$, and $n = 0.7$. It should be noted that E_{K_1} is kept constant. Therefore, E_{S_1} is varied to generate various E_{S_1}/E_{K_1} ratios. The curves in Fig. 4 show that the strain energy release rate decreases with increasing of E_{S_1}/E_{K_1} ratio (this behaviour is due to the increase of the beam stiffness). The strain energy release rate obtained assuming linear-elastic behaviour of the inhomogeneous material is also plotted in Fig. 4 for comparison with the non-linear solution. It should be noted that the linear-elastic solution for the strain energy release rate is derived by substituting of $H \rightarrow \infty$ in (2.26), (2.29), (2.31), (2.34)–(2.39) and (2.46)–(2.49) since at $H \rightarrow \infty$ the Ramberg-Osgood stress-strain relation (2.10) transforms into the Hooke's law. One can observe in Fig. 4 that the non-linear mechanical behaviour of the material leads to an increase of the strain energy release rate.

The effect of E_{T_1}/E_{K_1} ratio on the fracture behaviour is illustrated in Fig. 5 where the strain energy release rate in non-dimensional form is plotted against E_{T_1}/E_{K_1} ratio at three H/E_{K_1} ratios. In Fig. 5, it can be also observed that the strain energy release rate decreases with increasing of E_{T_1}/E_{K_1} and H/E_{K_1} ratios.

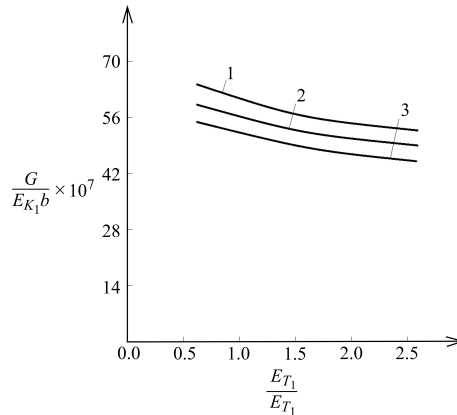


FIG. 5. The strain energy release rate in non-dimensional form presented as a function of E_{T_1}/E_{K_1} ratio (curve 1 – at $H/E_{K_1} = 0.5$, curve 2 – at $H/E_{K_1} = 2$ and curve 3 – at $H/E_{K_1} = 8$).

The influence of E_{K_2}/E_{K_1} ratio and the crack length on the crack behaviour is elucidated too. For this purpose, the strain energy release rate in non-dimensional form is plotted against a/l ratio at two E_{K_2}/E_{K_1} ratios in Fig. 6. The curves in Fig. 6 indicate that the strain energy release rate decreases with increasing the crack length when $E_{K_2}/E_{K_1} = 1.5$. This finding is attributed to the fact that the modulus of elasticity in the beam cross-section in which the crack front is located increases with increasing the crack length. One can also observe that at $E_{K_2}/E_{K_1} = 0.5$ the strain energy release rate increases with increasing the

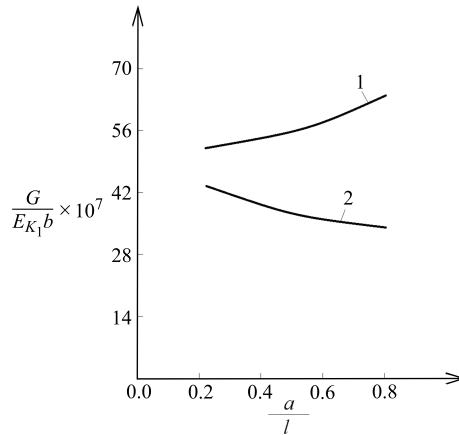


FIG. 6. The strain energy release rate in non-dimensional form presented as a function of a/l ratio (curve 1 – at $E_{K_2}/E_{K_1} = 0.5$ and curve 2 – at $E_{K_2}/E_{K_1} = 1.5$).

crack length (Fig. 6). The curves in Fig. 6 also show that the strain energy release rate at $E_{K_2}/E_{K_1} = 0.5$ is higher than that at $E_{K_2}/E_{K_1} = 1.5$ when $0.20 \leq a/l \leq 0.80$.

The distribution of the J -integral value along the crack front is shown in Fig. 7 at two E_{S_1}/E_{K_1} ratios and $a/l = 0.75$. The J -integral value is presented in non-dimensional form by using the formula $J_N = J/(E_{K_1}b)$. Calculations are carried out by applying (2.61). The abscise axis y_1/b in Fig. 7 is directed along the crack front (y_1/b is chosen such that its origin is located in the centre of the crack front).

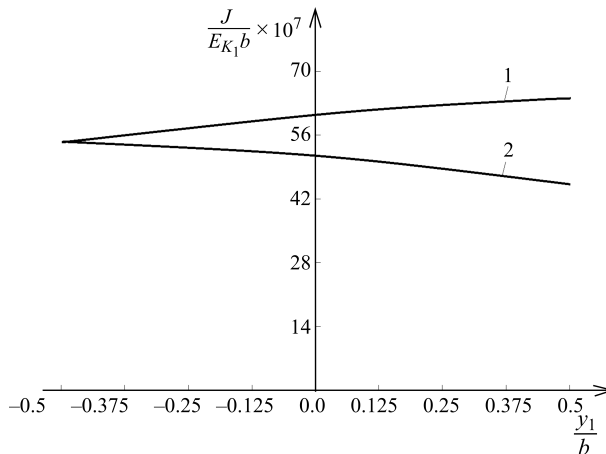


FIG. 7. Distribution of the J -integral value in non-dimensional form along the crack front (curve 1 – at $E_{S_1}/E_{K_1} = 0.5$ and curve 2 – at $E_{S_1}/E_{K_1} = 2.0$). The horizontal axis, y_1/b , is chosen such that $y_1/b = 0.0$ is located in the centre of the crack front.

Besides, $y_1/b = 0.5$ is on the lateral surface $S_1T_1S_2T_2$ of the beam (Fig. 1). The curves in Fig. 7 indicate that the J -integral value is distributed non-uniformly along the crack front. In Fig. 7, it can also be observed that the J -integral value increases with increasing of abscise, y_1/b , at $E_{S_1}/E_{K_1} = 0.5$. This finding is attributed to the fact that at $E_{S_1}/E_{K_1} = 0.5$ the modulus of elasticity decreases with increasing of y_1/b . At $E_{S_1}/E_{K_1} = 2.0$ the J -integral value decreases with increasing of y_1/b (Fig. 7). It should be noted that the distribution of the strain energy release rate along the crack front is the same as that of the J -integral shown in Fig. 7 since the J -integral is equal to the strain energy release rate [7]. The crack growth will initiate in the point of the crack front where the strain energy release rate is a maximum. Thus, the maximum strain energy release rate G_{\max} has to be compared with the critical strain energy release rate, G_C . The crack growth will initiate when $G_{\max} \geq G_C$. It should be mentioned that the critical strain energy release rate is a material property that is distributed non-uniformly along the crack front since the material is inhomogeneous. The distribution pattern of the critical strain energy release rate along the crack front is the same as that of the J -integral shown in Fig. 7.

Non-symmetric loading conditions (only the lower crack arm is loaded by a moment M_L , while the upper crack arm is free of stresses) are also considered. The strain energy release rate in non-dimensional form is plotted against M_L at two E_{T_1}/E_{K_1} ratios in Fig. 8. The curves in Fig. 8 show that the strain energy release rate increases quickly with increasing of M_L . It can be observed also that an increase of E_{T_1}/E_{K_1} ratio leads to a decrease of the strain energy release rate (Fig. 8).

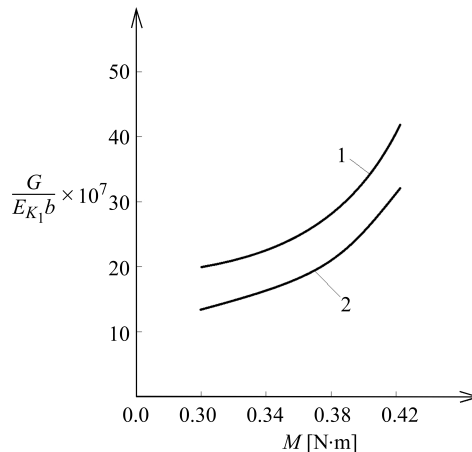


FIG. 8. The strain energy release rate in non-dimensional form presented as a function of M_L when only the lower crack arm is loaded (curve 1 – at $E_{T_1}/E_{K_1} = 0.5$ and curve 2 – at $E_{T_1}/E_{K_1} = 2.0$).

The curves in Figs 4–7 and 8 indicate that the inhomogeneous non-linear elastic beam under consideration can be optimised with respect to the strain energy release rate (for instance, by varying E_{S_1}/E_{K_1} , E_{T_1}/E_{K_1} , and H/E_{K_1} ratios the strain energy release rate can be significantly decreased, which improves the lengthwise crack performance of the beam).

The distribution of the normal stresses in non-dimensional form σ/E_{K_1} , along the height of the lower crack arm at $y_1 = 0$ in the cross-section of abscissa, $x_1 = a/3$, is presented in Fig. 9 at $E_{T_1}/E_{K_1} = 1.5$ (the coordinate system, $x_1 y_1 z_1$, is shown in Fig. 2). One can observe in Fig. 9 that the normal stresses are distributed non-uniformly along the height of the lower crack arm cross-section which is due to the non-linear mechanical behaviour of the material and to the material inhomogeneity. It can be observed also in Fig. 9 that the normal stress at the lower surface is higher than that of the upper surface of the crack arm (this finding is attributed to the fact that the value of the modulus of elasticity at the lower surface is higher than that at the upper surface of the crack arm). Figure 10 shows the distribution of the normal stresses in non-dimensional form

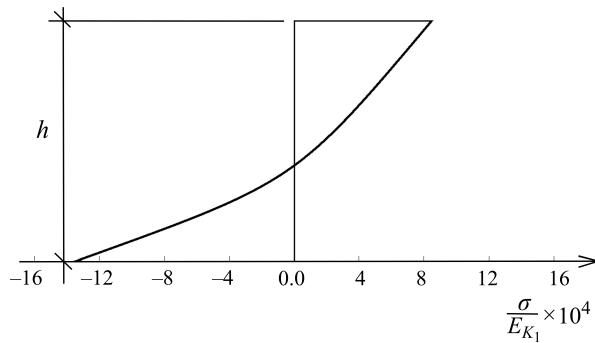


FIG. 9. Distribution of the normal stresses in non-dimensional form along the height of the lower crack arm at $y_1 = 0$ in the cross-section of abscissa, $x_1 = a/3$ (the coordinate system, $x_1 y_1 z_1$, is shown in Fig. 2).

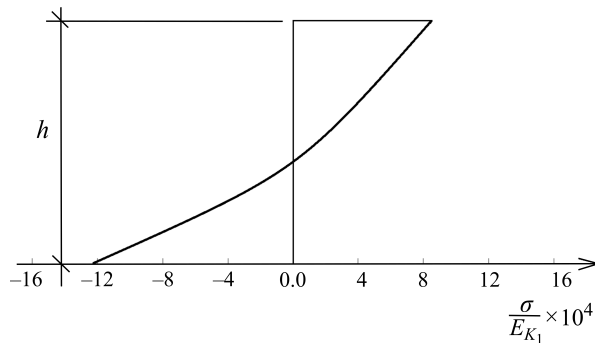


FIG. 10. Distribution of the normal stresses in non-dimensional form along the height of the lower crack arm at $y_1 = 0$ in the cross-section of abscissa, $x_1 = 2a/3$.

along the height of the lower crack arm at $y_1 = 0$ in the cross-section of abscissa, $x_1 = 2a/3$.

4. CONCLUSION

In the present paper, a technique for analyzing lengthwise crack in non-linear elastic beams exhibiting three-axial material inhomogeneity, i.e., inhomogeneity in width, height and length directions of the beam, is developed. It is assumed that the modulus of elasticity of the inhomogeneous material varies linearly along the width, height and length of the beam. The non-linear mechanical behaviour of the inhomogeneous material is modelled by using the Ramberg-Osgood stress-strain relation. A solution to the strain energy release rate is derived by analysing the energy balance. In order to verify the solution, the strain energy release rate is also obtained by using the complementary strain energy. A parametric study of lengthwise crack is performed to elucidate the effects of material inhomogeneity, material non-linearity and crack length on the crack behaviour. The material inhomogeneity along the width, height and length of the beam is characterised by E_{S_1}/E_{K_1} , E_{T_1}/E_{K_1} , and E_{K_2}/E_{K_1} ratios, respectively. The analysis revealed that the strain energy release rate decreases with increasing of E_{S_1}/E_{K_1} , E_{T_1}/E_{K_1} , and E_{K_2}/E_{K_1} ratios. It is found that the non-linear mechanical behaviour of the inhomogeneous material increases the strain energy release rate. Concerning the effect of crack length, it is found that the strain energy release rate increases with increasing the crack length when $E_{K_2}/E_{K_1} < 1$. If $E_{K_2}/E_{K_1} > 1$, the increase of the crack length leads to decrease of the strain energy release rate.

In addition, the J -integral approach is applied in the present paper. The distribution of the J -integral value along the crack front is analysed. It is found that the J -integral value (and the strain energy release rate) is distributed non-uniformly along the crack front which is due to the material inhomogeneity (this fact shows that the crack growth will initiate in the point of the crack front where the strain energy release rate is maximal). The technique developed in the present paper can be applied in crack-mechanics based structural design of beam structures made of non-linear elastic materials whose properties vary continuously along the width, height and length of the beam.

REFERENCES

1. TOKOVYY YU., MA C.-C., *Axisymmetric stresses in an elastic radially inhomogeneous cylinder under length-varying loadings*, ASME Journal of Applied Mechanics, **83**(11), 7 pages, 2016, doi: 10.1115/1.4034459.

2. TOKOVYY YU.V., RYCHAHIVS'KYI A.V., *Analytic solution of the plane problem of the theory of elasticity for a nonuniform strip*, Material Science, **41**(1): 135–138, 2005.
3. TOKOVYY YU., MA C.-C., *Three-dimensional temperature and thermal stress analysis of an inhomogeneous layer*, Journal of Thermal Stresses, **36**: 790–808, 2018, doi: 10.1080/01495739.2013.787853.
4. GASIK M.M., *Functionally graded materials: bulk processing techniques*, International Journal of Materials and Product Technology, **39**: 20–29, 2010.
5. BOHIDAR S.K., SHARMA R., MISHRA P.R., *Functionally graded materials: A critical review*, International Journal of Research, **1**(4): 289–301, 2014.
6. AL-HUNITI N.S., ALAHMAD S.T., *Transient thermo-mechanical response of a functionally graded beam under the effect of a moving heat source*, Advances in Materials Research, **6**(1): 27–43, 2017.
7. RIZOV V., *An analytical solution to the strain energy release rate of a crack in functionally graded beams*, European Journal of Mechanics – A/Solids, **65**(6): 301–312, 2017.
8. RIZOV V., *Fracture analysis of functionally graded beams with considering material non-linearity*, Structural Engineering and Mechanics, **64**(4): 487–494, 2017.
9. RIZOV V., *Analysis of longitudinal cracked two-dimensional functionally graded beams exhibiting material non-linearity*, Frattura ed Integrità Strutturale, **41**: 498–510, 2017.
10. LUBLINER J., *Plasticity Theory (Revised edition)*, University of California, Berkeley, CA, 2006.
11. RIZOV V.I., *Delamination in a two-dimensional functionally graded beam*, Journal of Applied Mechanics and Technical Physics, **59**: 146–152, 2018.
12. RIZOV V.I., *Delamination analysis of a layered elastic-plastic beam*, International Journal of Structural Integrity, **8**(5): 516–529, 2017.
13. HSUEH C.H., TUAN W.H., WEI W.C.J., *Analyses of steady-state interface fracture of elastic multilayered beams under four-point bending*, Scripta Materialia, **60**: 721–724, 2009.

Received April 16, 2018; accepted version December 4, 2018.

Published on Creative Common licence CC BY-SA 4.0

